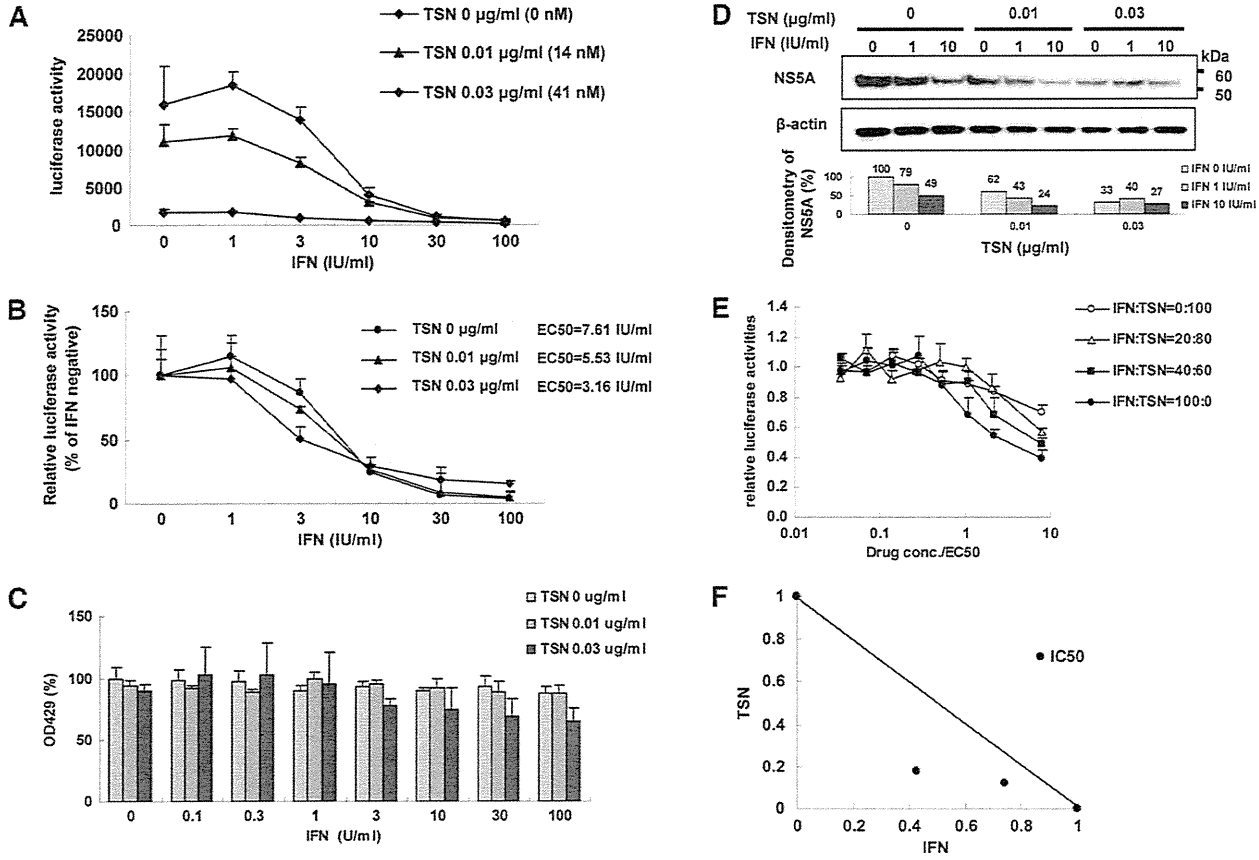

FIG. 4. Suppression of HCV RNA replication by TSN combined with α-IFN. (A and B) Luciferase activity (A, absolute value; B, relative value). Huh7/Rep-Feo cells, which constitutively express an HCV replicon, enable the quantification of replication levels through the measurement of luciferase activity. Absolute and relative dose-response curves in the presence of 24 h of pretreatment of various concentrations of TSN (0, 0.01, 0.03 μg/ml) and α-IFN (0, 100 IU/ml). (A) Bars indicate luciferase activities. (B) Bars indicate luciferase activities relative to the activity of each α-IFN-negative control. Luciferase assays were performed in triplicate. Error bars indicate means ± SDs. (C) MTS assay of Huh7/Rep-Feo cells cultured with the indicated concentrations of TSN and α-IFN. The assays were done in triplicate and repeated three times. Error bars indicate means ± SDs. (D) Western blotting. Ten micrograms of total cellular protein was separated by polyacrylamide gel electrophoresis and transferred onto the membrane. Monoclonal anti-NS5A antibody or an anti-beta-actin antibody was used as the primary antibody. Densitometry of NS5A or beta-actin protein was performed and the result is indicated as a percentage of that for the drug-negative control. The assay was repeated three times, and representative results are shown. (E) Dose-inhibition curves of α-IFN and TSN when they were combined at the indicated ratios, adjusted by the EC_{50} of the individual drug. Assays were done in triplicate, and mean values were plotted and indicated as means ± SDs. (F) Graphical representation of the isobologram analysis. For each drug combination in panel E, the EC_{50}s of α-IFN and TSN for inhibition of HCV replication were plotted against the fractional concentrations of α-IFN and TSN, which are indicated on the *x* and *y* axes, respectively. A theoretical line of additivity is drawn between the EC_{50} for each drug alone. All of the fractional EC_{50} plots for the TSN and α-IFN combinations fell below the line of additivity, indicating synergy.

the fractional EC_{50} of each drug ratio fell below the line showing additivity, indicating that the effect of the drug combination on intracellular HCV RNA replication was synergistic. The MTS values at the drug concentrations used in this isobologram analysis did not show any significant decrease, suggesting that the synergistic action of α-IFN and TSN on HCV replication is through their pharmacological effects and is not due to augmentation of cytotoxicity.

Suppression of HCV-J6/JFH1 infection by pretreatment of TSN with α-IFN. The inhibitory effects of pretreatment with TSN prior to α-IFN treatment demonstrated on HCV subgenomic replication were validated further using HCV-J6/JFH1 cell culture (21, 42). Various concentrations of TSN and α-IFN were added to HCV-J6/JFH1-infected Huh7 cells, and intracellular HCV RNA was quantified after 48 h of incubation. As shown in Fig. 5A, TSN with or without α-IFN suppressed expression of intracellular HCV RNA in a dose-dependent manner. The EC_{50}s of α-IFN with TSN at 0, 10, and 30 nM were 4.71 IU/ml, 3.83 IU/ml, and 3.52 IU/ml, respectively. An MTS-based cell viability assay did not show significant cytotoxicity from TSN (Fig. 5B). These data indicate that pretreatment with TSN also augmented the α-IFN effect on the JFH1 system.

TSN upregulates ISGF3 in combination with α-IFN. Subsequently, we performed experiments to investigate the mechanisms of action of TSN. First, we quantified expression of alpha/beta IFN receptor subunit (IFNAR) 1 and IFNAR2 and the effect of TSN. Real-time RT-PCR analysis showed no

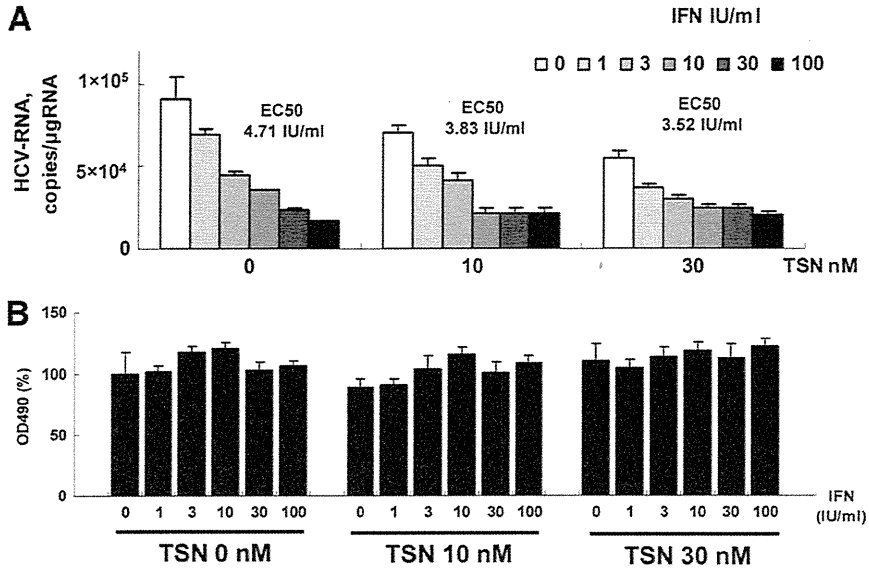

FIG. 5. Suppression of full HCV-J6/JFH1 replication by pretreatment of TSN with α-IFN. Ten micrograms of HCV-J6/JFH1 RNA was transfected into Huh7 cells. At 48 h after transfection, cells were pretreated with TSN for 24 h, followed by treatment with α-IFN (0, 1, 3, 10, 30, 100 IU/ml). At 48 h after α-IFN addition, cells were harvested. (A) Real-time RT-PCR analysis; (B) effect of pretreatment TSN with α-IFN on cell viability. MTS assays were performed 48 h after culture in the presence of pretreatment TSN with α-IFN. Bars indicate values relative to that of the drug-negative control. In panels A and B, the assays were done in triplicate and repeated three times. Error bars indicate means ± SDs.

change in levels of IFNAR1 and IFNAR2 mRNA expression with or without TSN (Fig. 6).

Next, we investigated the ISGF3 components, STAT1, and STAT2, using Western blotting, and interferon regulatory factor 9 (IRF9), using real-time RT-PCR. Huh7 cells were treated with various concentrations of TSN or 0.01% DMSO. Twenty-four hours after TSN treatment, 100 IU/ml of α-IFN was added, and STATs and IRF9 were detected. Western blot analysis demonstrated that phosphorylated STAT1 and STAT2 levels were increased more by treatment with α-IFN and TSN than by α-IFN treatment alone (Fig. 7A and B). In addition, IRF9 mRNA expression was significantly higher following pretreatment with TSN prior to α-IFN therapy than by α-IFN monotherapy (Fig. 8). These findings are consistent with the hypothesis that TSN activates ISGF3 components in combination with α-IFN.

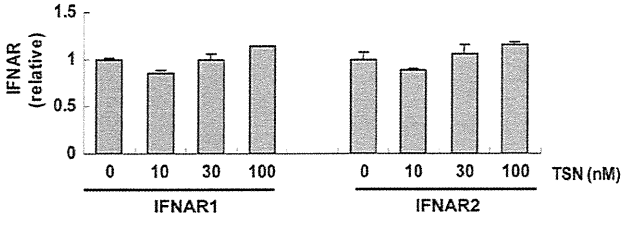

FIG. 6. IFNAR expression. Huh7 cells were pretreated with TSN for 24 h, followed by treatment with 100 IU/ml α-IFN for 6 h. The total cellular RNA was then isolated for real-time RT-PCR analysis of the mRNAs of IFNAR1 and IFNAR2. The assays were done in triplicate and repeated three times. The data are shown as means ± SDs.

DISCUSSION

In this study, we investigated the molecular actions of TSN on HCV replication and on α-IFN-mediated cellular antiviral responses. Treatment of cells expressing an HCV subgenomic replicon with TSN alone specifically inhibited HCV replication with a selectivity index of more than 146 (Fig. 2). In addition, pretreatment of cells with TSN prior to addition of α-IFN augmented α-IFN receptor-mediated, ISRE-regulated gene expression (Fig. 3). Consistent with these findings, TSN pretreatment significantly enhanced the suppressive effects of α-IFN on the HCV replicon and HCV cell culture (Fig. 4 and 5). Finally, we demonstrated that the α-IFN-enhancing effects of TSN are through increased transcriptional activation of a component of ISGF3 (Fig. 7 and 8). Taken together, out results demonstrate that TSN is potentially an effective antiviral agent when it is used alone and especially when it is used in combination with α-IFN and that screening for such α-IFN-enhancing agents may identify promising antiviral therapeutics. Because TSN treatment alone or simultaneous treatment with TSN and α-IFN did not increase ISRE activity or augment α-IFN-mediated ISRE activation, TSN may affect α-IFN sensitivity by upregulating molecules that affect α-IFN receptor-mediated signaling without activating ISRE signaling directly.

Type I interferon plays a central role in eliminating viruses through its innate antiviral activity or following therapeutic application. Binding of α-IFNs to their receptors activates the Jak-STAT pathway to form a complex with ISGF3, which translocates to the nucleus, binds the ISRE located in the promoter/enhancer region of the ISGs, and activates expression of ISGs (28, 39, 40). In this study, we demonstrated that TSN enhanced α-IFN effects by upregulating ISGF3, which

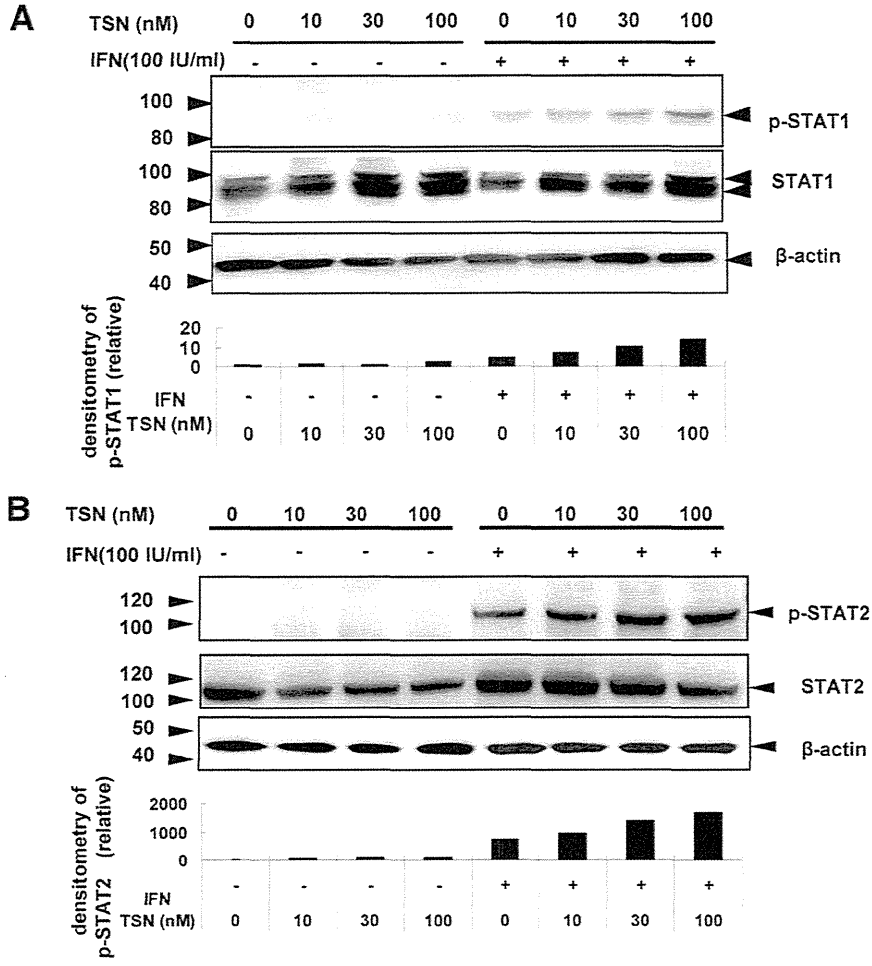

FIG. 7. TSN with α-IFN treatment of Huh7 cells increases phosphorylation of STAT1 and STAT2. (A) Western blotting. Alteration in the distribution of α-IFN-induced phosphorylation of STAT1 and STAT2 by TSN. Huh7 cells were treated with TSN or 0.01% DMSO for 24 h. After that, the cells were stimulated by 100 IU/ml α-IFN for 30 min. Cells were harvested, and the resulting lysates were analyzed for phosphorylated and total STAT1 or STAT2. The relative amounts of phosphorylated STAT1 or STAT2 were normalized to the amount of total STAT1 or STAT2 and expressed relative to the amount for the drug-negative control. The assay was repeated three times, and a representative result is shown.

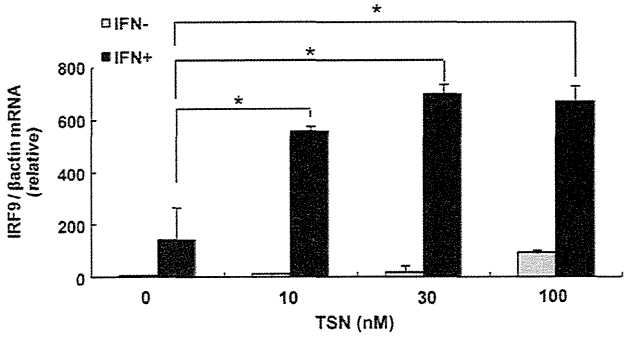

FIG. 8. IRF9 mRNA expression after combination treatment with TSN and α-IFN. Real-time RT-PCR analysis. Huh7 cells were treated with TSN for 24 h. After 6 h, the cells were stimulated by α-IFN (100 IU/ml). We used the method described in the legend to Fig. 6 to analyze the mRNA of IRF9. The assays were done in triplicate and repeated three times. Error bars indicate means ± SDs. *, $P < 0.05$.

may cancel the suppressive effect of HCV gene products on the α-IFN signaling pathway.

In our study, it was not proved that increasing ISRE activities had direct relevance to inhibition of HCV replication. In Fig. 3C, we showed that TSN with α-IFN treatment had elevated the level of expression of mRNA of ISGs. Previous studies suggested that overexpression of known ISGs inhibited HCV replication in HCV replicon-containing Huh7 cells (13, 14). These findings may support the possibility that TSN had the potential to augment the α-IFN effect.

Other than the canonical Jak/STAT-mediated α-IFN signaling pathway, several alternative α-IFN pathways have been reported, including the NF-kappaB, gamma IFN, PI3K, and MAPK pathways (9, 16, 24, 28). We carried out reporter assays using NF-kappaB, AP1, and GAS reporter plasmid constructs and treated the cells with TSN. As shown in Fig. 3D, TSN activated NF-kappaB-regulated gene expression significantly. NF-kappaB is a sequence-specific transcription factor which

regulates the expression of numerous cellular and viral genes and plays important roles in inflammation, innate immune responses, tumorigenesis, and cell survival (3, 19). Activation of NF-kappaB is principally regulated by tumor necrosis factor alpha (TNF-α), Toll-like receptors (TLRs), and RIG-I, which may possibly be associated with the molecular mechanisms of TSN monotherapy. Horsmans et al. (12) and Agrawal and Kandimalla (1) reported that TLR7, -8, and -9 agonists have the ability to modulate TLR-mediated immune responses in targeting a broad range of disease vectors, including HCV, alone or in combination with other therapeutic agents. These reports support the hypothesis that activation of NF-kappaB may be one of the mechanisms of action of TSN.

It has been reported that TSN exhibits cytotoxic/antiproliferative potential at high concentrations (36, 47). In our study, the selectivity index of TSN against HCV was sufficient to ascertain that the antiviral effects are not simply due to the cytotoxicity of TSN. A recent study showed that a triterpenoid compound, dammarenolic acid, inhibits retrovirus, human immunodeficiency virus, simian immunodeficiency virus, murine leukemia virus, and respiratory syncytial virus infections *in vitro* (4) (5). We have analyzed the effects of dammarenolic acid on antiviral actions on Huh7/Rep-Feo cells, cytotoxicity, and ISRE reporter activation. However, dammarenolic acid did not inhibit HCV replication or enhanced α-IFN-induced ISRE activity (data not shown). These findings suggest that the anti-HCV and α-IFN enhancer effects are distinctive features of TSN among triterpenoid compounds. Hiasa et al. have reported that ME3738, a triterpenoid saponin, suppressed HCV replication through production of endogenous beta interferon (11). ME3738 is now in clinical trials for treatment of HCV-infected patients. Taking these findings together, despite reports on the cell-suppressive effect of triterpenoids, properly selected or designed compounds might be used as drugs against HCV infection.

Because the mechanisms of action of these triterpenoid compounds against these viruses are poorly understood, further investigation of the mechanism of action of TSN on HCV may be valuable to implement antiviral strategies against other viruses. It would be important to assess drug resistance after continuous treatment with TSN. There is no *in vitro* or *in vivo* report on resistance of TSN or cellular attenuation of responses to TSN. Such information, if any is found, would help elucidate the mechanism of action of TSN.

Given the current situation of limited therapeutic options against HCV, the search for more potent and less toxic antiviral drugs is needed to improve clinical anti-HCV chemotherapeutics. Several direct antiviral agents with activity against HCV are currently undergoing clinical trials. These include NS3 protease inhibitors and NS5B polymerase inhibitors (41). However, the frequent emergence of drug-resistant viruses is a major weakness of such agents (20). Our results indicate that TSN is also effective at suppressing HCV infection and replication. Future studies with TSN, its derivatives, and other chemicals that target the α-IFN pathway could be directed toward developing a new class of antiviral treatment regimens and drugs.

ACKNOWLEDGMENTS

We thank Frank Chisari for providing Huh7.5.1 cells, Charles Rice for providing plasmid pJ6/JFH1full, and Takaji Wakita for providing plasmid pJFH1full.

This study was supported by grants from the Ministry of Education, Culture, Sports, Science and Technology of Japan, the Japan Society for the Promotion of Science, the Ministry of Health, Labor and Welfare of Japan, the Japan Health Sciences Foundation, the National Institute of Biomedical Innovation, and the Miyakawa Memorial Research Foundation.

REFERENCES

1. **Agrawal, S., and E. R. Kandimalla.** 2007. Synthetic agonists of Toll-like receptors 7, 8 and 9. Biochem. Soc. Trans. **35:**1461–1467.
2. **Bailey, M., N. A. Williams, A. D. Wilson, and C. R. Stokes.** 1992. PROBIT: weighted probit regression analysis for estimation of biological activity. J. Immunol. Methods **153:**261–262.
3. **Baldwin, A. S., Jr.** 2001. Series introduction: the transcription factor NF-kappaB and human disease. J. Clin. Invest. **107:**3–6.
4. **Esimone, C. O., et al.** 2008. Potential anti-respiratory syncytial virus lead compounds from Aglaia species. Pharmazie **63:**768–773.
5. **Esimone, C. O., et al.** Dammarenolic acid, a secodammarane triterpenoid from Aglaia sp. shows potent anti-retroviral activity in vitro. Phytomedicine **17:**540-547.
6. **Fried, M. W., et al.** 2002. Peginterferon alfa-2a plus ribavirin for chronic hepatitis C virus infection. N. Engl. J. Med. **347:**975–982.
7. **Funaoka, Y., et al.** Analysis of interferon signaling by infectious hepatitis C virus clones with substitutions of core amino acids 70 and 91. J. Virol., in press.
8. **Ge, D., et al.** 2009. Genetic variation in IL28B predicts hepatitis C treatment-induced viral clearance. Nature **461:**399–401.
9. **Goodbourn, S., L. Didcock, and R. E. Randall.** 2000. Interferons: cell signalling, immune modulation, antiviral response and virus countermeasures. J. Gen. Virol. **81:**2341–2364.
10. **Hadziyannis, S. J., et al.** 2004. Peginterferon-alpha2a and ribavirin combination therapy in chronic hepatitis C: a randomized study of treatment duration and ribavirin dose. Ann. Intern. Med. **140:**346–355.
11. **Hiasa, Y., et al.** 2008. Hepatitis C virus replication is inhibited by 22beta-methoxyolean-12-ene-3beta, 24(4beta)-diol (ME3738) through enhancing interferon-beta. Hepatology **48:**59–69.
12. **Horsmans, Y., et al.** 2005. Isatoribine, an agonist of TLR7, reduces plasma virus concentration in chronic hepatitis C infection. Hepatology **42:**724–731.
13. **Itsui, Y., et al.** 2009. Antiviral effects of the interferon-induced protein guanylate binding protein 1 and its interaction with the hepatitis C virus NS5B protein. Hepatology **50:**1727–1737.
14. **Itsui, Y., et al.** 2006. Expressional screening of interferon-stimulated genes for antiviral activity against hepatitis C virus replication. J. Viral Hepat. **13:**690–700.
15. **Jiang, D., et al.** 2008. Identification of three interferon-inducible cellular enzymes that inhibit the replication of hepatitis C virus. J. Virol. **82:**1665–1678.
16. **Kalvakolanu, D. V.** 2003. Alternate interferon signaling pathways. Pharmacol. Ther. **100:**1–29.
17. **Kanazawa, N., et al.** 2004. Regulation of hepatitis C virus replication by interferon regulatory factor 1. J. Virol. **78:**9713–9720.
18. **Karakama, Y., et al.** 2010. Inhibition of hepatitis C virus replication by a specific inhibitor of serine-arginine-rich protein kinase. Antimicrob. Agents Chemother. **54:**3179–3186.
19. **Karin, M., and A. Lin.** 2002. NF-kappaB at the crossroads of life and death. Nat. Immunol. **3:**221–227.
20. **Kuntzen, T., et al.** 2008. Naturally occurring dominant resistance mutations to hepatitis C virus protease and polymerase inhibitors in treatment-naive patients. Hepatology **48:**1769–1778.
21. **Lindenbach, B. D., et al.** 2005. Complete replication of hepatitis C virus in cell culture. Science **309:**623–626.
22. **Mishima, K., et al.** 2010. Cell culture and in vivo analyses of cytopathic hepatitis C virus mutants. Virology **405:**361–369.
23. **Nakagawa, M., et al.** 2005. Suppression of hepatitis C virus replication by cyclosporin a is mediated by blockade of cyclophilins. Gastroenterology **129:**1031–1041.
24. **Randall, R. E., and S. Goodbourn.** 2008. Interferons and viruses: an interplay between induction, signalling, antiviral responses and virus countermeasures. J. Gen. Virol. **89:**1–47.
25. **Sadler, A. J., and B. R. Williams.** 2008. Interferon-inducible antiviral effectors. Nat. Rev. Immunol. **8:**559–568.
26. **Sakamoto, N., and M. Watanabe.** 2009. New therapeutic approaches to hepatitis C virus. J. Gastroenterol. **44:**643–649.
27. **Sakamoto, N., et al.** 2007. Bone morphogenetic protein-7 and interferon-alpha synergistically suppress hepatitis C virus replicon. Biochem. Biophys. Res. Commun. **357:**467–473.

28. **Samuel, C.** 2001. Antiviral actions of interferons. Clin. Microbiol. Rev. **14:**778–809.
29. **Sangiovanni, A., et al.** 2006. The natural history of compensated cirrhosis due to hepatitis C virus: a 17-year cohort study of 214 patients. Hepatology **43:**1303–1310.
30. **Sekine-Osajima, Y., et al.** 2008. Development of plaque assays for hepatitis C virus-JFH1 strain and isolation of mutants with enhanced cytopathogenicity and replication capacity. Virology **371:**71–85.
31. **Shi, Y. L., and M. F. Li.** 2007. Biological effects of toosendanin, a triterpenoid extracted from Chinese traditional medicine. Prog. Neurobiol. **82:**1–10.
32. **Shi, Y. L., and Z. F. Wang.** 2004. Cure of experimental botulism and antibotulismic effect of toosendanin. Acta Pharmacol. Sin. **25:**839–848.
33. **Soothill, J. S., R. Ward, and A. J. Girling.** 1992. The IC50: an exactly defined measure of antibiotic sensitivity. J. Antimicrob. Chemother. **29:**137–139.
34. **Suda, G., et al.** IL-6-mediated intersubgenotypic variation of interferon sensitivity in hepatitis C virus genotype 2a/2b chimeric clones. Virology **407:**80–90.
35. **Suppiah, V., et al.** 2009. IL28B is associated with response to chronic hepatitis C interferon-alpha and ribavirin therapy. Nat. Genet. **41:**1100–1104.
36. **Tada, K., M. Takido, and S. Kitanaka.** 1999. Limonoids from fruit of Melia toosendan and their cytotoxic activity. Phytochemistry **51:**787–791.
37. **Tanabe, Y., et al.** 2004. Synergistic inhibition of intracellular hepatitis C virus replication by combination of ribavirin and interferon-alpha. J. Infect. Dis. **189:**1129–1139.
38. **Tanaka, Y., N. Nishida, M. Sugiyama, K. Tokunaga, and M. Mizokami.** Lambda-interferons and the single nucleotide polymorphisms: a milestone to tailor-made therapy for chronic hepatitis C. Hepatol. Res. **40:**449–460.
39. **Taniguchi, T., K. Ogasawara, A. Takaoka, and N. Tanaka.** 2001. IRF family of transcription factors as regulators of host defense. Annu. Rev. Immunol. **19:**623–655.
40. **Taniguchi, T., and A. Takaoka.** 2002. The interferon-alpha/beta system in antiviral responses: a multimodal machinery of gene regulation by the IRF family of transcription factors. Curr. Opin. Immunol. **14:**111–116.
41. **Thompson, A. J., and J. G. McHutchison.** 2009. Antiviral resistance and specifically targeted therapy for HCV (STAT-C). J. Viral Hepat. **16:**377–387.
42. **Wakita, T., et al.** 2005. Production of infectious hepatitis C virus in tissue culture from a cloned viral genome. Nat. Med. **11:**791–796.
43. **Yokota, T., et al.** 2003. Inhibition of intracellular hepatitis C virus replication by synthetic and vector-derived small interfering RNAs. EMBO Rep. **4:**602–608.
44. **Zeuzem, S., et al.** 2000. Peginterferon alfa-2a in patients with chronic hepatitis C. N. Engl. J. Med. **343:**1666–1672.
45. **Zhang, B., Z. F. Wang, M. Z. Tang, and Y. L. Shi.** 2005. Growth inhibition and apoptosis-induced effect on human cancer cells of toosendanin, a triterpenoid derivative from Chinese traditional medicine. Invest. New Drugs **23:**547–553.
46. **Zhang, J. H., T. D. Chung, and K. R. Oldenburg.** 1999. A simple statistical parameter for use in evaluation and validation of high throughput screening assays. J. Biomol. Screen. **4:**67–73.
47. **Zhang, Y., et al.** 2008. Roles of reactive oxygen species and MAP kinases in the primary rat hepatocytes death induced by toosendanin. Toxicology **249:**62–68.
48. **Zhong, J., et al.** 2005. Robust hepatitis C virus infection in vitro. Proc. Natl. Acad. Sci. U. S. A. **102:**9294–9299.

Biochemical and Biophysical Research Communications 406 (2011) 134–140

Contents lists available at ScienceDirect

Biochemical and Biophysical Research Communications

journal homepage: www.elsevier.com/locate/ybbrc

Cholestatic liver fibrosis and toxin-induced fibrosis are exacerbated in matrix metalloproteinase-2 deficient mice

Izumi Onozuka [a,1], Sei Kakinuma [a,b,*,1], Akihide Kamiya [c], Masato Miyoshi [d], Naoya Sakamoto [a,b], Kei Kiyohashi [a], Takako Watanabe [a], Yusuke Funaoka [a], Mayumi Ueyama [a], Mina Nakagawa [a], Naohiko Koshikawa [e], Motoharu Seiki [e], Hiromitsu Nakauchi [c], Mamoru Watanabe [a,*]

[a] Department of Gastroenterology and Hepatology, Tokyo Medical and Dental University, Japan
[b] Department for Hepatitis Control, Tokyo Medical and Dental University, Japan
[c] Division of Stem Cell Therapy, Institute of Medical Science, The University of Tokyo, Japan
[d] School of Medicine, Tokyo Medical and Dental University, Japan
[e] Division of Cancer Cell Research, Institute of Medical Science, The University of Tokyo, Japan

ARTICLE INFO

Article history:
Received 25 January 2011
Available online 12 February 2011

Keywords:
Bile duct ligation
Carbon tetrachloride
PDGF receptor
TIMP1
TGFβ

ABSTRACT

Matrix metalloproteinase (MMP) plays an important role in homeostatic regulation of the extracellular environment and degradation of matrix. During liver fibrosis, several MMPs, including MMP-2, are up-regulated in activated hepatic stellate cells, which are responsible for exacerbation of liver cirrhosis. However, it remains unclear how loss of MMP-2 influences molecular dynamics associated with fibrogenesis in the liver. To explore the role of MMP-2 in hepatic fibrogenesis, we employed two fibrosis models in mice; toxin (carbon tetrachloride, CCl4)-induced and cholestasis-induced fibrosis. In the chronic CCl4 administration model, MMP-2 deficient mice exhibited extensive liver fibrosis as compared with wild-type mice. Several molecules related to activation of hepatic stellate cells were up-regulated in MMP-2 deficient liver, suggesting that myofibroblastic change of hepatic stellate cells was promoted in MMP-2 deficient liver. In the cholestasis model, fibrosis in MMP-2 deficient liver was also accelerated as compared with wild type liver. Production of tissue inhibitor of metalloproteinase 1 increased in MMP-2 deficient liver in both models, while transforming growth factor β, platelet-derived growth factor receptor and MMP-14 were up-regulated only in the CCl4 model. Our study demonstrated, using 2 experimental murine models, that loss of MMP-2 exacerbates liver fibrosis, and suggested that MMP-2 suppresses tissue inhibitor of metalloproteinase 1 up-regulation during liver fibrosis.

1. Introduction

The incidence of liver cirrhosis and cirrhosis-related cancer has steadily increased. Insight into the pathophysiology of hepatic fibrogenesis and fibrolysis is of particular importance. Accumulating evidences has indicated that matrix metalloproteinases (MMPs) play an essential role in hepatic fibrogenesis [1]. Traditional substrates of MMPs are components of the extracellular matrix (ECM), such as collagen, laminin, and fibronectin [2]. More than 20 enzymes have been identified as MMPs in mammals. In healthy liver, homeostasis of the ECM is maintained by precisely regulated turnover controlled by MMPs and tissue inhibitors of metalloproteinases (TIMPs) [1]. Hepatic stellate cells activated in chronically damaged liver disrupt this regulation by synthesizing a large amount of ECM, including collagen and proteoglycan, followed by production of MMPs and TIMPs [3]. It has been reported that the hepatic expression of MMP-1, -2, -7 and -14 is steadily increased with disease progression, and that the expression of MMP-9, -11 and -13 is transiently elevated in hepatitis C virus-induced cirrhosis [4]. Up-regulation of MMPs and TIMPs during liver fibrogensis has been observed in rodent models of liver fibrosis. In chronic toxin (carbon tetrachloride, CCl4)-induced rat liver fibrosis, production of MMP-2, -9, and -14 is increased during the accumulation of fibrotic scarring in the liver, and hepatic stellate cells

Abbreviations: ALT, alanine aminotransferase; αSMA, α smooth muscle actin; AST, aspartate aminotransferase; BDL, bile duct ligation; CCl4, carbon tetrachloride; ECM, extracellular matrix; GGT, γ-glutamyltranspeptidase; MMP, matrix metalloproteinase; MMP-2 KO, MMP-2 deficient; PDGF, platelet-derived growth factor; T-Bil, total bilirubin; TIMP, tissue inhibitor of metalloproteinase; TGF, transforming growth factor; WT, wild type .

* Corresponding authors at: Department of Gastroenterology and Hepatology, Tokyo Medical and Dental University, 1-5-45 Yushima, Bunkyo-ku, Tokyo 1138519, Japan. Fax: +81 3 5803 0268.

E-mail addresses: skakinuma.gast@tmd.ac.jp (S. Kakinuma), mamoru.gast@tmd.ac.jp (M. Watanabe).

[1] These authors contributed equally to this study.

0006-291X/$ - see front matter © 2011 Elsevier Inc. All rights reserved.
doi:10.1016/j.bbrc.2011.02.012

appear to be the predominant source [5–7]. MMPs degrade the ECM, and yet loss of MMP activity does not always induce fiborogenesis *in vivo*, because MMP functions are associated with regulation of several inflammatory cytokines [8].

MMP-2 is a 72-kDa zinc-dependent type IV collagenase, and the activation of proMMP-2 is controlled by MMP-14 and TIMP2 [9]. In the rat CCl4-induced fibrosis model, expression of MMP-2 increase up to 7–12 times as compared with that of controls, with the expression rate being maximal at an intermediate stage of fibrosis [5]. During the aggressive phase of CCl4-induced liver fibrosis, MMP-2 is predominantly produced from myofibroblasts derived from hepatic stellate cells [7]. MMP-2 expression has been shown to increase during spontaneous recovery from cirrhosis in a rat toxin-induced fibrosis model [10]. The proteolytic activity of MMP-2 is increased in cholestasis-induced liver fibrosis models in rats and mice [6,11]. These studies indicate that MMP-2 regulates both liver fibrogensis and fibrolysis. However, it remains unclear how MMP-2 functions during hepatic fibrogenesis in the liver *in vivo*, and the functional correlations between MMP and TIMP expression with liver fibrogenesis has not yet been fully elucidated.

In this study, to clarify the pivotal role of MMP-2 during liver fibrosis, we studied fibrotic changes in the liver of MMP-2 deficient (MMP-2 KO) mice using two types of fibrosis models; toxin (CCl4)-induced fibrosis and cholestasis-induced fibrosis. In both models, liver fibrosis was accelerated in MMP-2 KO mice as compared with wild type (WT) littermates. Type I collagen expression and TIMP1 production were up-regulated in MMP-2 KO livers in both models. Our data indicated that MMP-2 plays an essential role in suppressing fibrotic changes in the liver arising from chemical or cholestatic damage.

2. Materials and methods

2.1. Animals

MMP-2 deficient (MMP-2 KO) mice on C57BL/6J background were originally generated by Itoh et al. [12]. MMP-2 KO mice and wild type (WT) littermates were produced by crossbreeding MMP-2 heterozygous mice. All animals were treated under the guidelines of the Institute of Medical Science, University of Tokyo and those of Tokyo Medical and Dental University.

2.2. Liver fibrosis induced by chronic CCl4 administration

To induce hepatic fibrosis in mice, 6-week-old female MMP-2 KO and WT mice ($n = 4$ per group) were intraperitoneally injected with 10% CCl4 (2 ml/kg body weight, Wako Pure Chemical Industries, Osaka, Japan) dissolved in olive oil (Wako) twice weekly for 12 weeks. Negative control mice were injected with 100% olive oil alone twice weekly for 12 weeks.

2.3. Liver fibrosis induced by bile duct ligation (BDL)

To induce fibrosis by cholestasis, 8-week-old female MMP-2 KO and WT mice ($n = 4$ per group) underwent common bile duct ligation under anesthesia as previously described [13]. Mice were sacrificed 2 weeks after the operation.

2.4. Blood biochemical tests

Peripheral blood of MMP-2 KO and WT mice in the BDL group was collected and assayed for total bilirubin (T-Bil), alanine aminotransferase (ALT), aspartate aminotransferase (AST), and γ-glutamyltranspeptidase (GGT) using a Fuji DRI-Chem 3000 system (Fujifilm, Tokyo, Japan).

2.5. Immunohistological analysis

Fresh livers were snap-frozen in OCT compound and sectioned 8-μm thick. The protocols for immunostaining has been described previously [14]. Immunohistological analysis was performed using mouse anti-α smooth muscle actin (αSMA) antibody (Sigma, St. Louis, MO, USA). For each analysis, addition of an appropriate immune serum provided a negative control.

2.6. Western blot analyses

Samples of liver tissue were homogenized in RIPA buffer. The protocols for western blot analyses have been described previously [15]. Western blot analyses were performed with liver homogenates (50 μg protein) using anti-αSMA Ab (Sigma, 1:2000 dilution), anti-MMP9 antibody (Chemicon, Billerica, MA, USA, 1:1000 dilution), anti-MMP14 antibody (Abcam, Cambridge, MA, USA, 1:500 dilution), anti-TIMP1 antibody (Abcam, 1:1000 dilution), anti-TIMP2 antibody (Cell Signaling, Danvers, MA, USA, 1:500 dilution), or anti-β-actin antibody. Membrane pictures of immunoblots were quantified using ImageJ software (http://rsb.info.nih.gov/ij/).

Supplementary materials and methods are described in supplementary file.

3. Results

3.1. CCl4-induced hepatic fibrosis in MMP-2 KO mice

We initially studied liver fibrosis induced by chronic CCl4 administration in WT and MMP-2 KO mice. To induce extensive liver fibrosis, CCl4 was injected twice weekly for 12 weeks. Damage of hepatocytes in MMP-2 KO livers was very severe (Fig. S1). Sirius red staining of KO livers demonstrated that CCl4-induced fibrosis was severe in comparison with WT livers (Fig. 1A). Marked porto-central and porto-portal fibrosis was observed in the liver of MMP-2 KO mice treated with CCl4. The fibrosis areas, quantified using an image analysis system, were significantly increased in MMP-2 KO livers as compared with WT livers (Fig. 1B). Following chronic CCl4 administration, a 2-fold increase in fibrosis area was observed in MMP-2 KO livers as compared with WT livers.

3.2. Increased hepatic production of αSMA in MMP-2 KO mice treated with CCl4

To assess whether the activation of hepatic stellate cells is promoted in MMP-2 KO mice with CCl4-induced liver fibrosis, we examined hepatic αSMA production, which is a representative marker for myofibroblasts. Immunohistological analysis showed that αSMA-positive areas in the liver were much larger in CC14-treated MMP-2 KO mice than in CC14-treated WT mice (Fig. 1C). αSMA-positive areas quantified using an image analysis system were significantly increased in MMP-2 KO livers (Fig. 1D). Immunoblot analysis indicated that αSMA production was markedly increased in the livers of CCl4-treated WT and MMP-2 KO mice as compared with vehicle (olive oil)-treated WT and MMP-2 KO mice, respectively. Hepatic αSMA production was higher in CCl4-treated MMP-2 KO mice as compared with CCl4-treated WT mice (Fig. 1E). Quantitative analysis using densitometry demonstrated that hepatic level of αSMA protein was significantly higher in CCl4-treated MMP-2 KO mice than in CCl4-treated WT mice (Fig. 1F). These data suggest that the activation of hepatic stellate cells was promoted in MMP-2 KO liver as compared with WT liver during liver fibrosis induced by chronic CCl4 administration.

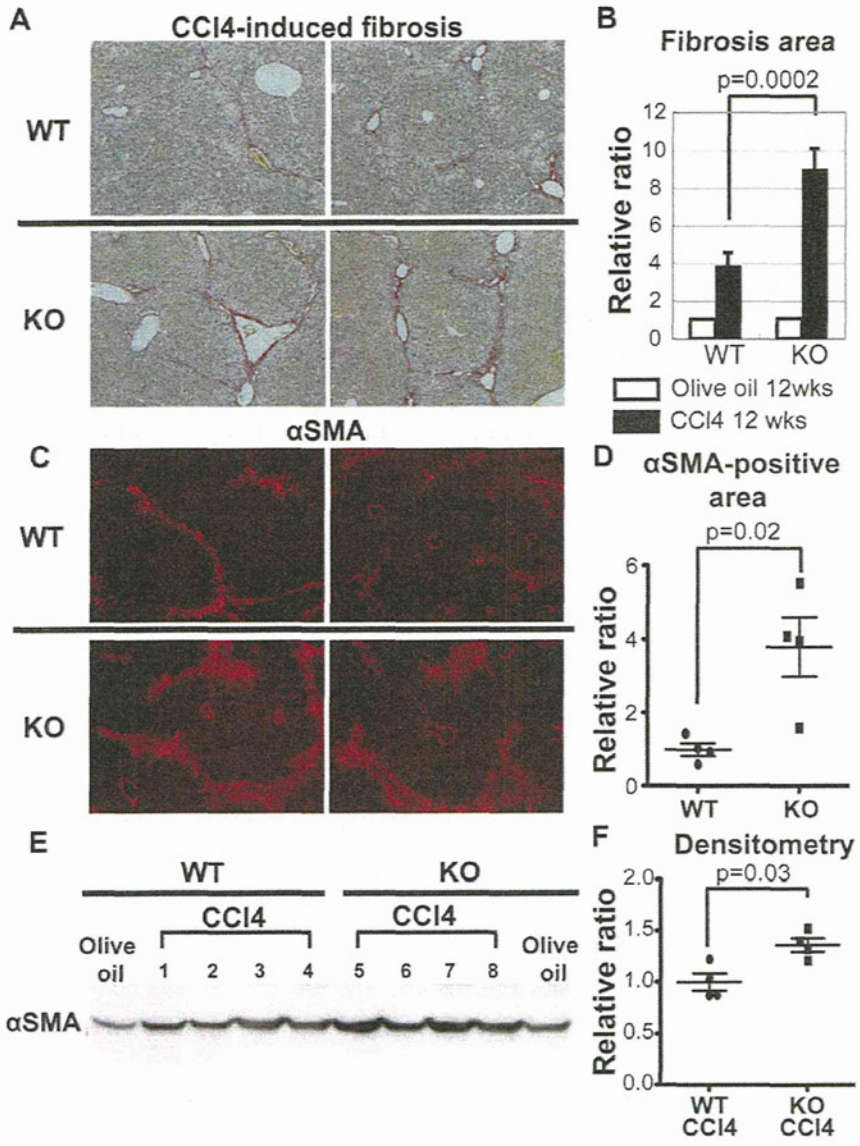

Fig. 1. CCl4-induced liver fibrosis is promoted in MMP-2 deficient (KO) mice. (A) Representative photographs of Sirius red staining in the livers of CCl4-treated mice. (B) Ratio of overall fibrosis area (red areas in Sirius red staining) relative to olive oil-treated WT mice. Data represent means ± SD. (C) Representative images of αSMA immunostaining in the livers of CCl4-treated mice. (D) Areas immunostained with αSMA antibody, quantified using an image analysis system, were significantly increased in CCl4-treated MMP-2 KO mice as compared with WT mice. Values represent the ratio relative to the mean for CCl4-treated WT mice. Bars represent means ± SEM. (E) Immunoblot analysis of αSMA in the liver of MMP-2 KO and WT mice. Mice 1, 2, 3, and 4 were CCl4-treated WT. Mice 5, 6, 7, and 8 were CCl4-treated MMP-2 KOs. (F) Hepatic αSMA protein quantified using densitometry was significantly increased in CCl4-treated MMP-2 KO mice as compared with WT mice. Values represent the ratio relative to the mean for CCl4-treated WT mice. Bars represent means ± SEM.

3.3. Hepatic expression of fibrosis-related molecules in CCl4-treated MMP-2 KO mice

To explore the molecular mechanism underlying the differences between WT and MMP-2 KO mice in response to CCl4-induced fibrosis, we analyzed the expression of molecules related to the promotion of liver fibrosis. Quantitative RT-PCR analysis showed that the hepatic expression of type I collagen in CCl4-treated MMP-2 KO mice was 4-fold higher than that in CCl4-treated WT mice (Fig. 2A). In addition, hepatic expression of transforming growth factor (TGF) β1 and platelet-derived growth factor (PDGF) receptor was up-regulated in CCl4-treated MMP-2 KO mice, whereas that of TGFβ receptor was comparable between CCl4-treated MMP-2 KO mice and CCl4-treated WT mice (Fig. 2A).

Immunoblot analysis showed that hepatic levels of MMP-9, MMP-14, TIMP1, and TIMP2 protein were increased in CCl4-treated WT mice relative to vehicle-treated mice, indicating that production of fibrosis-related molecules was up-regulated in our experimental model (Fig. 2B). Production of MMP-9, MMP-14, TIMP1 and TIMP2 in the liver was comparable between vehicle-treated WT mice and vehicle-treated KO mice (Fig. 2B). Quantitative analysis using densitometry also showed that hepatic production of MMP-14 and TIMP1 was significantly higher in CCl4-treated MMP-2 KO mice than in CCl4-treated WT mice (Fig. 2C). Hepatic

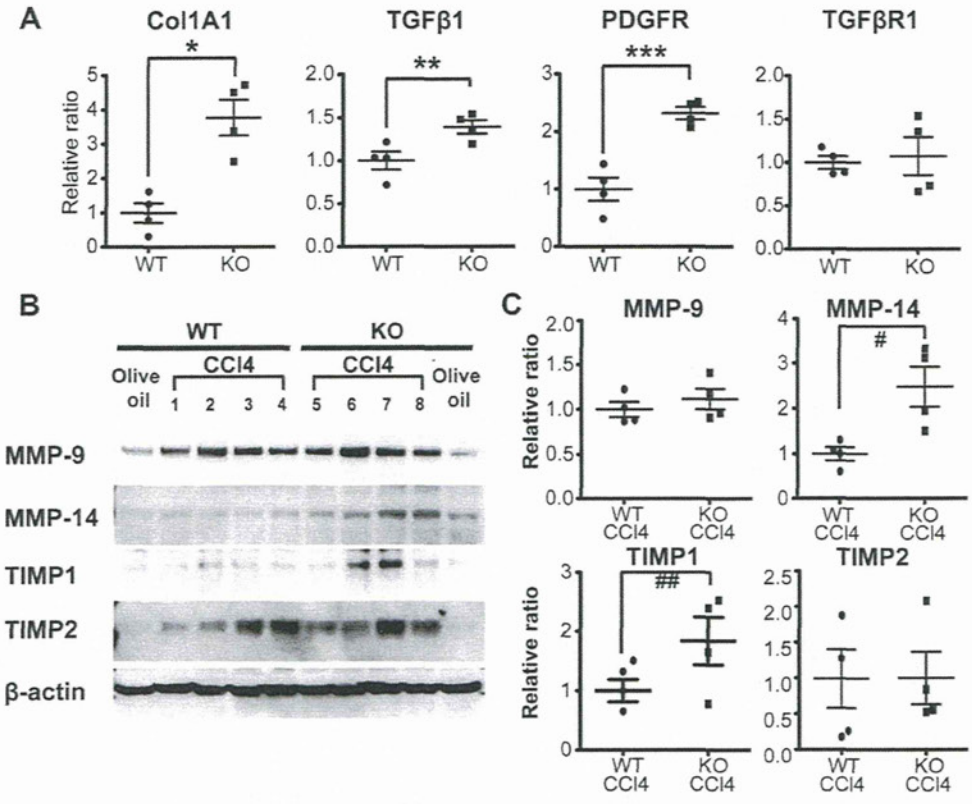

Fig. 2. Analysis of fibrosis-related molecules in the liver of CCl4-treated MMP-2 KO and WT mice. (A) Relative expression of type I collagen (Col1A1), TGFβ1, PDGF receptor (PDGFR), and TGFβ receptor 1 (TGFβR1). Test samples were normalized to the copy number for β-actin, with equal copies applied as templates. Col1A1, TGFβ1, and PDGFR were significantly up-regulated in MMP-2 KO liver as compared with WT liver. $^{*}P = 0.008$. $^{**}P = 0.02$. $^{***}P = 0.006$. (B) Immunoblot assays of MMP-9, MMP-14, TIMP1, and TIMP2. (C) Quantitative analysis using densitometry. Production of MMP-14 and TIMP1 in the liver was increased in CCl4-treated MMP-2 KO mice as compared with CCl4-treated WT mice. $^{\#}P = 0.01$. $^{\#\#}P = 0.03$. Values represent the ratio relative to the mean for CCl4-treated WT mice. Bars represent means ± SEM. The result is representative of 3 independent experiments.

production of MMP-9 and TIMP2 in CCl4-treated KO mice was almost equal to that in CCl4-treated WT mice (Fig. 2C). These data indicated that molecules related to stellate cell activation and fibrosis were up-regulated in CCl4-treated MMP-2 KO livers as compared with CCl4-treated WT livers, suggesting that loss of MMP-2 promoted the activation of hepatic stellate cells during CCl4-induced liver fibrosis.

3.4. Enhanced cholestatic fibrosis in MMP-2 KO mouse liver

Cholestatic fibrosis induced by BDL in MMP-2 KO and WT mice was analyzed at 2-weeks post-induction. Blood biochemical testing showed severe hyperbilirubinemia in mice treated with BDL (Table S2). The serum level of GGT was significantly higher in BDL-treated MMP-2 KO mice as compared with BDL-treated WT mice, whereas no significant change in T-Bil, AST, and ALT was found in either group (Table S2). Microscopic analysis of liver specimens showed extensive bile ductule proliferation and peribiliary fibrosis in BDL-treated mice (Fig. 3A). Bile ductule proliferation was more severe in BDL-treated MMP-2 KO mice than in BDL-treated WT mice (Fig. 3A). Sirius red staining analysis demonstrated more severe BDL-induced peribiliary fibrosis in KO mice than in WT mice (Fig. 3B). The fibrosis areas, quantified using an image analysis system, were significantly increased in BDL-treated KO mice as compared with BDL-treated WT mice (Fig. 3C). There was no difference in hepatic fibrosis area between WT and MMP-2 KO sham-operated mice (Fig. S2). This data indicated that cholestasis-induced liver fibrosis was exacerbated in MMP-2 KO mice as compared with WT mice.

3.5. Hepatic αSMA production in MMP-2 KO mice with BDL-induced fibrosis

Hepatic αSMA production was assessed to determine changes in hepatic myofibroblasts associated with cholestasis-induced fibrosis. The size of αSMA-positive areas in the liver did not differ significantly between WT and MMP-2 KO sham-operated mice (Fig. S3A). Hepatic αSMA in BDL-treated mice was detected in periportal regions only. The αSMA-positive area in the liver of BDL-treated MMP-2 KO mice was almost equal to that of BDL-treated WT mice (Fig. S3A). As well as immunostaining analysis, immunoblot analysis showed that hepatic αSMA production in BDL-treated MMP-2 KO mice was almost equal to that in BDL-treated WT mice (Fig. 3D). Quantitative analyses using an image analysis system and densitometry also showed that hepatic αSMA production in BDL-treated MMP-2 KO mice was not significantly increased relative to WT mice (Figs. S3B and 3E).

3.6. Expression of fibrosis-related molecules in MMP-2 KO mice with cholestasis-induced fibrosis

The hepatic expression of molecules related to the promotion of liver fibrosis was studied in MMP-2 KO and WT mice with BDL-treated fibrosis. Quantitative RT-PCR analysis showed that hepatic

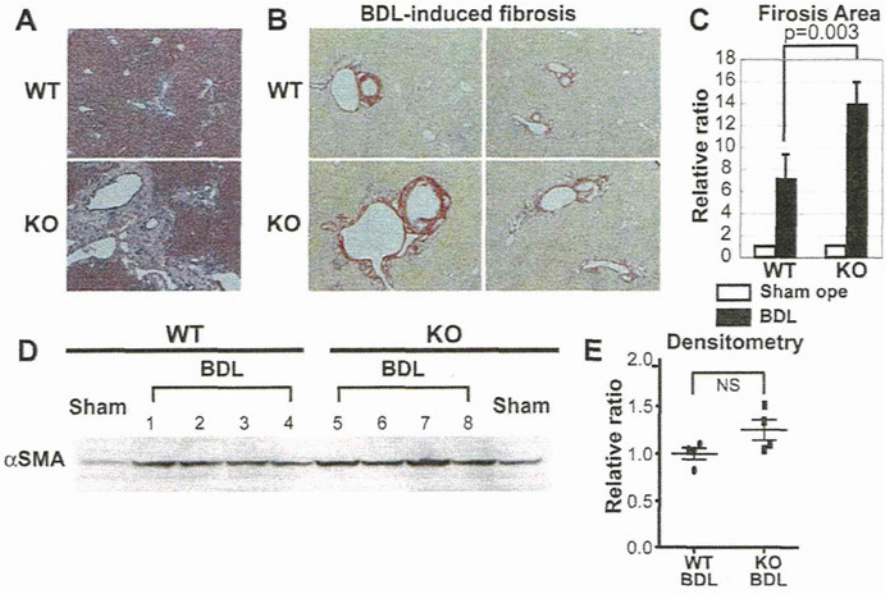

Fig. 3. Cholestasis-induced liver fibrosis is accelerated in MMP-2 KO mice. MMP-2 KO mice and WT littermates ($n = 4$ per group) were subjected to bile duct ligation (BDL). Negative control mice were sham operated (Sham). (A) Hematoxylin eosin staining of liver specimens of BDL-treated mice. (B) Representative photographs of Sirius red staining in the liver of BDL-treated mice. (C) Ratio of overall fibrosis area relative to sham-operated WT mice. Data represent means ± SD. (D) Immunoblot analysis of αSMA in the liver of MMP-2 KO and WT mice. (E) Quantitative analysis of αSMA using densitometry. The αSMA protein in the immunoblot analysis was unchanged. Values represent the ratio relative to the mean for BDL-treated WT mice. Bars represent means ± SEM.

expression of type I collagen, TIMP1, MMP-9, MMP-14, PDGF receptor, and TGFβ was up-regulated in BDL-treated mice as compared with sham-operated mice (Figs. 4A and S4). Hepatic expression of type I collagen in BDL-treated KO mice was 2-fold higher than that in BDL-treated WT mice (Fig. 4A). The hepatic expression of TIMP1 was also up-regulated in BDL-treated KO mice (Fig. 4A). However, there was no significant difference in the hepatic expression of MMP-9, MMP-14, TGFβ, TGFβ receptor, or PDGF receptor between BDL-treated KO and BDL-treated WT mice (Figs. 4A and S4).

Immunoblot analysis showed that the levels of MMP-9, MMP-14, TIMP1 and TIMP2 protein in the liver were higher in BDL-treated mice as compared with sham-operated mice, indicating that production of fibrosis-related molecules was up-regulated in our experimental model (Fig. 4B). Quantitative analysis using densitometry showed that hepatic TIMP1 production was significantly higher in BDL-treated KO mice than BDL-treated WT mice (Fig. 4C). There was no significant difference in the production of MMP-9, MMP-14, or TIMP2 between BDL-treated KO mice and BDL-treated WT mice. Our data indicated that type I collagen and TIMP1 was up-regulated in BDL-treated MMP-2 KO mice as compared with WT mice, suggesting that TIMP1 production is related to acceleration of cholestasis-induced fibrosis in the liver of MMP-2 KO mice.

4. Discussion

In the present study, we analyzed liver fibrosis and fibrosis-related molecules in MMP-2 KO mice in models of toxin- and cholestasis-induced fibrosis. This is the first study to show that BDL-induced hepatic fibrosis is accelerated in MMP-2 KO mice, and that the expression of type I collagen is increased (Figs. 3C and 4A). BDL duplicates the hepatocytic damage, activation of hepatic stellate cells, and liver fibrosis observed in human liver disease. In the early phase of BDL, there is a marked and transient proliferation of bile duct epithelial cells associated with proliferation of portal periductular fibroblasts which rapidly express αSMA [16]. This supports the hypothesis that portal myofibroblasts play an important role in BDL-induced fibrogenesis. Myofibroblastic differentiation of portal fibroblasts is mediated by several signaling pathways including the TGFβ [17] and PDGF [18] pathways. Our data indicate that these molecules were up-regulated in the liver of BDL-treated mice as compared with sham-operated mice, in consistent with previous reports. Hepatic αSMA production in MMP-2 KO mice was almost equal to that of WT mice (Fig. 3E), and the hepatic expression of TGFβ1, TGFβ receptor, and PDGF receptor in BDL-treated MMP-2 KO liver was unchanged in comparison with BDL-treated WT liver (Figs. 4A and S4). Taken together, our data suggest that the myofibroblastic differentiation of portal fibroblasts in KO liver was almost equal to that of WT liver.

Hepatic TIMP1 was up-regulated in BDL-treated MMP-2 KO mice as compared with BDL-treated WT mice (Figs. 4A and 4C), indicating that loss of MMP-2 in cholestatic liver induces the TIMP1 production. In BDL-induced liver fibrosis, TIMP1 is expressed in myofibroblasts. However, loss of TIMP1 activity does not result in improvement of liver fibrosis as indicated by a previous study in TIMP1/TIMP2 double-KO mice, which showed that TIMP1 and TIMP2 do not play an essential role in experimental hepatic fibrogenesis by schistosomiasis [19]. The mechanism of TIMP1 up-regulation in MMP-2 KO liver remains unclear; however, it is possible that the ability of MMP-2-deficient portal fibroblasts to suppress TIMP1 production is impaired due to lack of MMP-2-mediated signaling. Further study is necessary to address this issue.

Previous studies have indicated that hepatic stellate cells undergo an activation process, acquire a fibroblastic phenotype, express αSMA, and play a major role in collagen deposition in CCl4-induced liver fibrosis [1,20]. TGFβ induces the production of type I collagen in activated hepatic stellate cells. PDGF receptor is up-regulated in activated hepatic stellate cells proliferating in response to PDGF. Progression of CCl4-induced liver fibrosis is

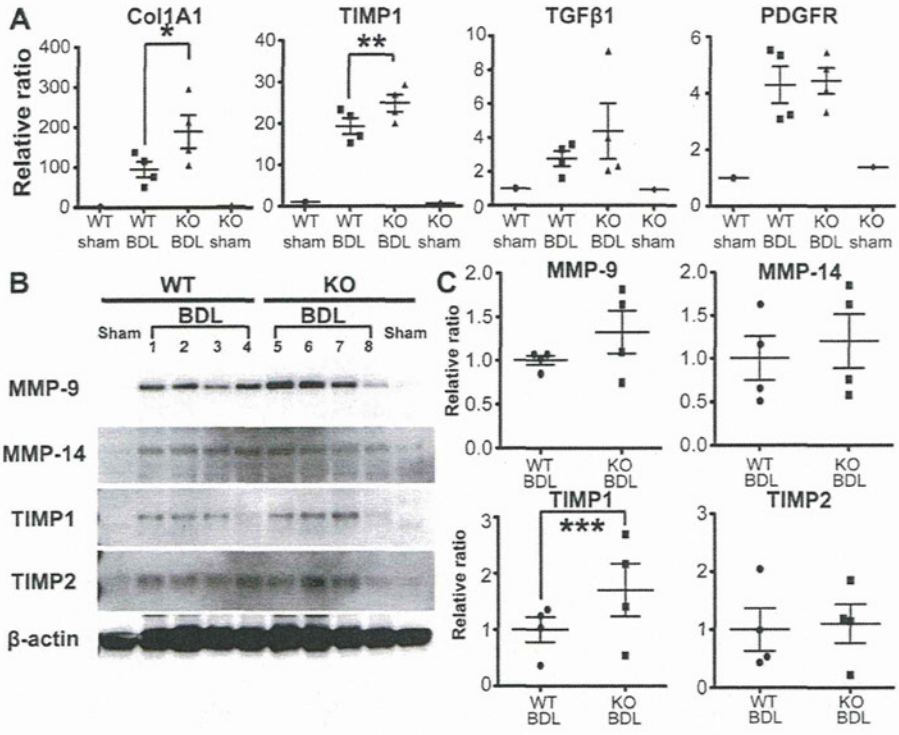

Fig. 4. Analysis of fibrosis-related molecules in the liver of BDL-treated mice. (A) Relative expression of Col1A1, TIMP1, TGFβ1, and PDGFR. Test samples were normalized to the copy number for β-actin, with equal copies applied as templates. Hepatic expression of Col1A1 and TIMP1 was significantly up-regulated in BDL-treated MMP-2 KO mice as compared with BDL-treated WT mice. Values represent the ratio relative to the mean for sham-operated WT mice. (B) Immunoblot assays of MMP-9, MMP-14, TIMP1, and TIMP2. (C) Quantitative analysis using densitometry. Hepatic production of TIMP1 in BDL-treated MMP-2 KO mice was increased as compared with BDL-treated WT mice. Values represent the ratio relative to the mean for BDL-treated WT mice. Bars represent means ± SEM. $^{*}P = 0.02$. $^{**}P = 0.003$. $^{***}P = 0.04$. The result is representative of 3 independent experiments.

mediated by these molecules. Our data suggest that activation of hepatic stellate cells was promoted in MMP-2 KO mice as compared with WT mice. This is supported by the observation that the production of αSMA and TIMP1 was increased in MMP-2 KO liver (Figs. 1 and 2), because the activated hepatic stellate cells (myofibroblasts) are a major source of TIMP1 [21]. Thus, our data suggest the activation of hepatic stellate cells was promoted by loss of MMP-2 activity *in vivo*. Previous research has shown that loss of MMP-2 amplifies CCl4-induced liver fibrosis, but no increase was seen in the *in vivo* levels of several molecules related to activation of hepatic stellate cells [22]. This discrepancy may be due to the duration of chronic CCl4 administration, which was twice as long in our study. Increased hepatic levels of MMP-14 protein in CCl4-treated MMP-2 KO mice may be due to a compensatory effect for MMP-2 deficiency, which is generally activated by MMP-14.

Classical substrates of MMPs are components of the ECM; however, the list of substrates has been extended to include various receptors, ligands and adhesion molecules [2]. Several studies have demonstrated changes in the hepatic fibrotic response in MMP-deficient mice. Madala et al. reported that chronic helminth-induced liver fibrosis was attenuated in MMP-12 deficient mice. MMP-12 deficiency is associated with up-regulation of ECM-degrading enzymes such as MMP-2, -9, and -13 in Th2 cytokine-driven fibrosis [23]. Furthermore, loss of ECM-degrading MMPs does not always lead to progression of liver fibrosis. MMP-13 is one of the representative ECM-degrading enzymes in mice. In the liver of BDL-treated MMP-13 KO mice, activation of hepatic stellate cells was paradoxically suppressed in comparison with WT mice [8], suggesting that MMP-13 probably contributes to accelerating fibrogenesis in cholestatic livers by mediating inflammation rather than promoting fibrolysis. On the other hand, our data showed that MMP-2 contributes to suppression of fibrogenesis in both toxin- and cholestasis-induced liver damage. One possible interpretation is that MMP-2-mediated signaling is associated with the suppression of inflammation or fibrosis, which influence the production of type I collagen and TIMP1 derived from myofibroblasts. Another is that MMP-2 simply contributes to acceleration of fibrolysis. Radbill et al. showed that the expression of type I collagen in cultured hepatic stellate cells was decreased by knockdown of MMP-2 [22], suggesting that MMP-2-mediated signals directly regulate the expression of type I collagen. Thus, development of specific activators of MMP-2, but not of other ECM-degrading enzymes, could be promising as a new therapeutic strategy for the treatment of liver cirrhosis.

Acknowledgments

This work was supported in part by Grants-in-Aid for Scientific Research from the Ministry of Education, Culture, Sports, Science and Technology in Japan, the Ministry of Health, Labor and Welfare in Japan, the Japan Society for the Promotion of Science, Japan Health Sciences Foundation, National Institute of Biomedical Innovation, and the Foundation for Advancement of International Science. We thank Dr. S. Itohara for providing us MMP-2 deficient mice. We thank Prof. Y. Inagaki and Dr. T. Moro in Tokai University for helpful discussions about the method for bile duct ligation. We also thank Y. Wakiyama, K. Okada, K. Itoh, H. Itoh, and A. Yanagida in Division of Stem Cell Therapy, Institute of Medical Science, University of Tokyo for excellent technical assistance.

Appendix A. Supplementary data

Supplementary data associated with this article can be found, in the online version, at doi:10.1016/j.bbrc.2011.02.012.

References

[1] S. Hemmann, J. Graf, M. Roderfeld, et al., Expression of MMPs and TIMPs in liver fibrosis – a systematic review with special emphasis on anti-fibrotic strategies, J. Hepatol. 46 (2007) 955–975.
[2] M. Seiki, The cell surface: the stage for matrix metalloproteinase regulation of migration, Curr. Opin. Cell Biol. 14 (2002) 624–632.
[3] S.L. Friedman, Evolving challenges in hepatic fibrosis, Nat. Rev. Gastroenterol. Hepatol. 7 (2010) 425–436.
[4] R. Lichtinghagen, M.J. Bahr, M. Wehmeier, et al., Expression and coordinated regulation of matrix metalloproteinases in chronic hepatitis C and hepatitis C virus-induced liver cirrhosis, Clin. Sci. 105 (2003) 373–382.
[5] T. Takahara, K. Furui, J. Funaki, et al., Increased expression of matrix metalloproteinase-II in experimental liver fibrosis in rats, Hepatology 21 (1995) 787–795.
[6] A.E. Kossakowska, D.R. Edwards, S.S. Lee, et al., Altered balance between matrix metalloproteinases and their inhibitors in experimental biliary fibrosis, Am. J. Pathol. 153 (1998) 1895–1902.
[7] T. Watanabe, M. Niioka, A. Ishikawa, et al., Dynamic change of cells expressing MMP-2 mRNA and MT1-MMP mRNA in the recovery from liver fibrosis in the rat, J. Hepatol. 35 (2001) 465–473.
[8] H. Uchinami, E. Seki, D.A. Brenner, et al., Loss of MMP 13 attenuates murine hepatic injury and fibrosis during cholestasis, Hepatology 44 (2006) 420–429.
[9] M. Seiki, N. Koshikawa, I. Yana, Role of pericellular proteolysis by membrane-type 1 matrix metalloproteinase in cancer invasion and angiogenesis, Cancer Metastasis Rev. 22 (2003) 129–143.
[10] R. Issa, X. Zhou, C.M. Constandinou, et al., Spontaneous recovery from micronodular cirrhosis: evidence for incomplete resolution associated with matrix cross-linking, Gastroenterology 126 (2004) 1795–1808.
[11] Y. Osawa, Y.A. Hannun, R.L. Proia, et al., Roles of AKT and sphingosine kinase in the antiapoptotic effects of bile duct ligation in mouse liver, Hepatology 42 (2005) 1320–1328.
[12] T. Itoh, T. Ikeda, H. Gomi, et al., Unaltered secretion of beta-amyloid precursor protein in gelatinase A (matrix metalloproteinase 2)-deficient mice, J. Biol. Chem. 272 (1997) 22389–22392.
[13] E.L. Opie, M.B. Rothbard, Osmotic homeostasis maintained by mammalian liver, kidney, and other tissues, J. Exp. Med. 97 (1953) 483–497.
[14] S. Kakinuma, H. Ohta, A. Kamiya, et al., Analyses of cell surface molecules on hepatic stem/progenitor cells in mouse fetal liver, J. Hepatol. 51 (2009) 127–138.
[15] S. Kakinuma, Y. Tanaka, R. Chinzei, et al., Human umbilical cord blood as a source of transplantable hepatic progenitor cells, Stem Cells 21 (2003) 217–227.
[16] J.A. Dranoff, R.G. Wells, Portal fibroblasts: underappreciated mediators of biliary fibrosis, Hepatology 51 (2010) 1438–1444.
[17] Z. Li, J.A. Dranoff, E.P. Chan, et al., Transforming growth factor-beta and substrate stiffness regulate portal fibroblast activation in culture, Hepatology 46 (2007) 1246–1256.
[18] N. Kinnman, C. Francoz, V. Barbu, et al., The myofibroblastic conversion of peribiliary fibrogenic cells distinct from hepatic stellate cells is stimulated by platelet-derived growth factor during liver fibrogenesis, Lab. Invest. 83 (2003) 163–173.
[19] B. Vaillant, M.G. Chiaramonte, A.W. Cheever, et al., Regulation of hepatic fibrosis and extracellular matrix genes by the response: new insight into the role of tissue inhibitors of matrix metalloproteinases, J. Immunol. 167 (2001) 7017–7026.
[20] K. Wake, "Sternzellen" in the liver: perisinusoidal cells with special reference to storage of vitamin A, Am. J. Anat. 132 (1971) 429–462.
[21] E. Roeb, E. Purucker, B. Breuer, et al., TIMP expression in toxic and cholestatic liver injury in rat, J. Hepatol. 27 (1997) 535–544.
[22] B.D. Radbill, R. Gupta, M.C. Ramirez, et al., Loss of matrix metalloproteinase-2 amplifies murine toxin-induced liver fibrosis by upregulating collagen I expression, Dig. Dis. Sci. 56 (2011) 406–416.
[23] S.K. Madala, J.T. Pesce, T.R. Ramalingam, et al., Matrix metalloproteinase 12-deficiency augments extracellular matrix degrading metalloproteinases and attenuates IL-13-dependent fibrosis, J. Immunol. 184 (2010) 3955–3963.

Hepatology Research

Hepatology Research 2011; **41**: 258–269 doi: 10.1111/j.1872-034X.2010.00771.x

Original Article

Studies on virus kinetics using infectious fluorescence-tagged hepatitis C virus cell culture

Machi Yamamoto,[1]* Naoya Sakamoto,[1,2]* Tetsuya Nakamura,[1,3] Yasuhiro Itsui,[1,5] Mina Nakagawa,[1,2] Yuki Nishimura-Sakurai,[1] Sei Kakinuma,[1,2] Seishin Azuma,[1] Kiichiro Tsuchiya,[1] Takanobu Kato,[4] Takaji Wakita[4] and Mamoru Watanabe[1]

[1]*Department of Gastroenterology and Hepatology,* [2]*Department for Hepatitis Control,* [3]*Department of Advanced Therapeutics in Gastrointestinal Diseases, Tokyo Medical and Dental University,* [4]*Department of Virology II, National Institute of Infectious Disease, Tokyo, and* [5]*Department of Internal Medicine, Soka Municipal Hospital, Saitama, Japan*

Aim: Studies of the complete hepatitis C virus (HCV) life cycle have become possible with the development of a HCV-JFH1 cell culture system.

Methods: In this study, we constructed two fluorescence protein-tagged recombinant JFH1 virus clones, JFH1-EYFP and JFH1-AsRed, as well as two corresponding clones with adaptive mutations, JFH1-EYFP mutant and JFH1-AsRed mutant, that and were as effective as JFH1 in producing infectious virus particles, and investigated their viral infection life cycles.

Results: After infection of the fluorescence-tagged mutant viruses, infected cells increased exponentially. In cells, EYFP or AsRed and NS5A were expressed as a fusion protein and co-localized in core proteins. The rate of the cell–cell spread was dependent on the cell densities with a maximum of $10^{2.5}$/day. Treatment of cells with interferon or a protease inhibitor suppressed expansion of virus-positive cells.

Conclusion: Taken together, these results indicate that fluorescence-tagged HCV is a useful tool to study virus infection life cycles and to assist in the search for novel antiviral compounds.

Key words: AsRed, confocal laser microscopy, HCV-JFH1 cell culture, protease inhibitor, yellow fluorescence protein

INTRODUCTION

HEPATITIS C VIRUS (HCV) infection is characterized frequently by chronic inflammation of the liver, leading to decompensated liver cirrhosis and hepatocellular cancers.[1] Interferon (IFN)-α has been the mainstay of HCV therapy.[2] However, the most effective therapy, pegylated IFN plus ribavirin in combination, can eliminate HCV from only half of the patients treated[3,4] and often is accompanied by substantial side-effects.[5,6] These difficulties in eliminating the virus are attributable mostly to the limited treatment options.[7]

Correspondence: Dr Naoya Sakamoto, Department of Gastroenterology and Hepatology, Tokyo Medical and Dental University, 1-5-45 Yushima, Bunkyo-ku, Tokyo 113-8519, Japan. Email: nsakamoto.gast@tmd.ac.jp

*M. Y. and N. S. contributed equally to this work.

Received 15 July 2010; revised 21 November 2010; accepted 12 December 2010.

Hepatitis C virus belongs to the family Flaviviridae. The viruses have positive-strand RNA genomes of approximately 10 kb that encode polyproteins of approximately 3000 amino acids. The protein is post-translationally processed by cellular and viral proteases into at least 10 mature proteins. The viral non-structural (NS) proteins accumulate in the endoplasmic reticulum (ER) and they direct genomic replication and viral protein synthesis.[8,9] Studies of the HCV life cycle and the development of new drugs have long been hampered by the lack of cell culture systems. These problems have been greatly overcome by the development of the HCV subgenomic replicon[10] and HCV-JFH1 cell culture[11] systems.

After the development of HCV-JFH1 cell culture, many variations of reporter protein-tagged HCV systems have been described.[12–15] These reporter systems, however, feature poor or absent virus propagation, secretion and re-infection. The C-terminal end of the NS5A region, which has been used for insertion of

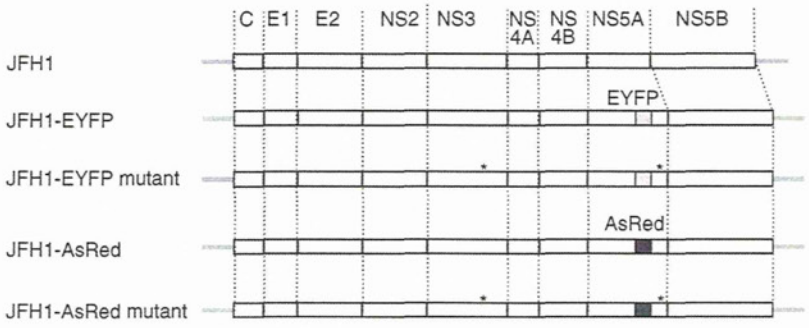

Figure 1 Schematic of the JFH1-based hepatitis C virus constructs. EYFP or AsRed was inserted in-frame into the *Cpo*I site of NS5A (JFH1-EYFP or JFH1-AsRed). The adaptive mutations in NS3 and NS5A (T4209A and C7653T) are indicated by asterisks (JFH1-EYFP mutant or JFH1-AsRed mutant).

reporter sequences, does not affect viral genomic replication,[12] while manipulation of the domain resulted in the loss of viral particle secretion possibly through abrogation of NS5A-core protein–protein association that is crucial for the viral particle assembly.[16] These problems have made it to difficult to analyze the entire viral life cycle in living cells. Recently, Han *et al.* reported a mutant HCV-JFH1 clone that expressed green fluorescent protein (GFP)-tagged NS5A and which could propagate and secrete infectious virus particles.[17]

In this study, we took advantage of the mutant fluorescence protein-tagged HCV and investigated the life cycles of HCV infection. We have demonstrated the rate of expansion of HCV infection using flow cytometry. Moreover, we have shown the kinetics of co-infection with two virus strains, which differed in their ability to secrete infectious virus particles.

METHODS

Reagents

RECOMBINANT HUMAN IFN-α-2b was from Schering-Plough (Kenilworth, NJ). Protease inhibitor (BILN2061) was from Boehringer Ingelheim (Ingelheim, Germany). BILN2061 is a macrocyclic NS3 protease inhibitor, the antiviral effects of which have been reported in a phase I clinical study.[18] Although further development of BILN2061 has been abandoned, this compound has structural homology with other protease inhibitors that are currently being evaluated in clinical trials, such as TMC435 and MK7009.[7,19]

Cell culture

Huh7.5.1 cells[20] and their derivatives were maintained in Dulbecco's modified minimal essential medium (DMEM; Sigma, St Louis, MO, USA) with 10% fetal bovine serum (FBS; Invitrogen, San Diego, CA, USA) at 37°C under 5% CO_2.

Plasmid constructs (Fig. 1)

In order to produce pJFH1-EYFP, the EYFP gene was amplified from pEYFP-C1 (Clontech, Mountain View, CA, USA) by polymerase chain reaction (PCR). The PCR products were then inserted into the *Cpo*I site (7484) of pJFH1. Similarly, pJFH1-AsRed was produced using pAsRed2 (Clontech). The JFH1-EYFP and JFH1-AsRed mutants, which are JFH1-based mutants with robust virus production capability, have two point mutations (T4209A, C7653T).[17] In order to introduce these mutations into pJFH1-AsRed, the *Avr*II/*Nsi*I and *Bsr*GI fragments of pJFH1-AsRed were amplified by PCR. The PCR products were subcloned into the T-Vector (pGEM-T Easy Vector Systems; Promega, Madison, WI, USA) and the mutations were introduced by site-directed mutagenesis (Quick-Change II Site-Directed Mutagenesis Kit; Stratagene, La Jolla, CA, USA), as reported previously.[21] Finally, these *Avr*II/*Nsi*I and *Bsr*GI fragments were reinserted into the parental plasmid, pJFH1-AsRed. The pJFH1-AsRed mutant was digested with *Cpo*I and the DNA fragment was subcloned into pJFH1-EYFP, producing the mutant pJFH1-EYFP. All nucleotide numbers refer to pJFH1.[11]

Constitutive expression of ER-fluorescence protein in Huh7.5.1 cells

Huh7.5.1 cells were seeded into 6-cm diameter dishes and transfected with pDsRed2-ER (Invitrogen) using Lipofectamine 2000 (Invitrogen) according to the manufacturer's protocol. Isolated clones (ER-Huh7.5.1 cells) were maintained under selection with 0.75 mg/mL G418 (Nacalai Tesque, Kyoto, Japan) and

screened for DsRed protein expression using fluorescence microscopy (BZ-8000; Keyence, Tokyo, Japan).

RNA transcription and transfection

Recombinant HCV RNA was synthesized and transfected as previously described.[22,23] Briefly, the plasmids were linearized by digestion with *XbaI* and subjected to *in vitro* transcription using RiboMax Large Scale RNA Production System (Promega). For the RNA transfection, Huh7.5.1 cells were suspended in Opti-MEM (Invitrogen) containing 10 μg of HCV RNA, transferred into a 4-mm electroporation cuvette, and subjected to an electric pulse (1050 μF and 270 V) using the Gene Pulser II apparatus (Bio-Rad, Richmond, CA, USA). After electroporation, the cell suspension was left for 5 min at room temperature and then incubated under normal culture conditions in a 10-cm diameter dish. The transfected cells were split every 3–5 days. The culture media were transferred subsequently onto uninfected Huh7.5.1 cells.

Immunofluorescence microscopy

Immunofluorescence microscopy was performed as described previously.[24] Cells were cultured on 18-mm round cover slips (Matsunami, Osaka, Japan) and fixed using 4% paraformaldehyde for 10 min at room temperature. Cells were incubated with the primary antibodies for 1 h at 37°C and with Alexa Fluor 488 goat antimouse immunoglobulin (Ig)G antibody (Molecular Probes, Eugene, OR, USA) for 1 h at room temperature in the dark. Mouse anti-NS5A antibody (Biodesign, Saco, ME, USA) and mouse anti-core antibody (Abcam, Cambridge, MA, USA) were used as primary antibodies. Cells were mounted with VECTA SHIELD Mounting Medium with DAPI (Vector Laboratories, Burlingame, CA, USA) and visualized by confocal laser fluorescent microscopy (BZ-8000 [Keyence] and FLUOVIEW FV10i [Olympus, Tokyo, USA]).[25]

Flow cytometry

JFH1-EYFP and JFH1-EYFP mutant-transfected Huh7.5.1 cells and uninfected Huh7.5.1 cells were cultured in 12-well plates (Becton Dickinson, Franklin Lakes, NJ, USA). The cells were collected on the days, post-transfection or post-infection, indicated. After washing with phosphate buffered saline (PBS; Nacalai Tesque) supplemented with 3% FBS and staining of dead cells with propidium iodide, the cells were analyzed using a FACS Calibur with CellQuest software (Becton Dickinson).

Quantification of HCV core antigen in the culture medium

The culture media from Huh7.5.1 cells transfected with JFH1 and its derivatives were collected on the days indicated and stored at 80°C. The levels of core antigen in the culture media were measured using a chemiluminescence enzyme immunoassay (CLEIA) according to the manufacturer's protocol (Lumipulse Ortho HCV Antigen; Ortho-Clinical Diagnostics).

Western blotting

Western blotting was carried out as described previously.[21] Briefly, 10 μg of total cell lysate was separated by sodium dodecylsulfate polyacrylamide gel electrophoresis and blotted onto a polyvinylidene fluoride membrane. The membrane was incubated with primary antibodies followed by peroxidase-labeled anti-IgG antibody and visualized by chemiluminescence using the ECL Western blotting Analysis System (Amersham Biosciences). The antibodies used were anti-core mouse monoclonal antibody 2H9, anti-NS5A mouse monoclonal antibody 9E10 (provided by Dr Rice), and anti-GFP rabbit polyclonal antibody (Invitrogen). The anti-GFP is able to detect EYFP. To confirm expression of EGFP in Huh 7.5.1 cells, Huh7.5.1 cells were seeded into a 6-cm diameter dish and transfected with pEGFP (Invitrogen) using Lipofectamine 2000 (Invitrogen).

Statistical analyses

Statistical analyses were performed using Welch's *t*-test. *P*-values of less than 0.05 were considered statistically significant.

Figure 2 Infectious hepatitis C virus (HCV) reporter virus with robust virus production capability. (a) Huh7.5.1 cells were transfected with JFH1-EYFP, JFH1-EYFP mutant, JFH1-AsRed or JFH1-AsRed mutant HCV RNA. At 3 days post-transfection, culture media were collected and added onto uninfected cells. At the days indicated, EYFP or AsRed-directed-fluorescence was visualized directly. (b) The ratio of EYFP or AsRed-positive cells in (a) is counted in each image and plotted vs time. Assays were carried out in triplicate and the results are expressed as mean ± standard deviation. $^*P < 0.05$. —●—, JFH1-EYFP mutant; ·◇·, JFH1-EYFP; —▲—, JFH1-AsRed mutant; ·△·, JFH1-AsRed. (c) The levels of core antigen in the culture medium of JFH1, JFH1-EYFP, JFH1-EYFP mutant, JFH1-AsRed, and JFH1-AsRed mutant-transfected Huh7.5.1 cells collected on the days indicated. Ag, antigen. ·●·, JFH1; ·◇·, JFH1-EYFP; —●—, JFH1-EYFP mutant; ·△·, JFH1-AsRed; —▲—, JFH1-AsRed mutant.

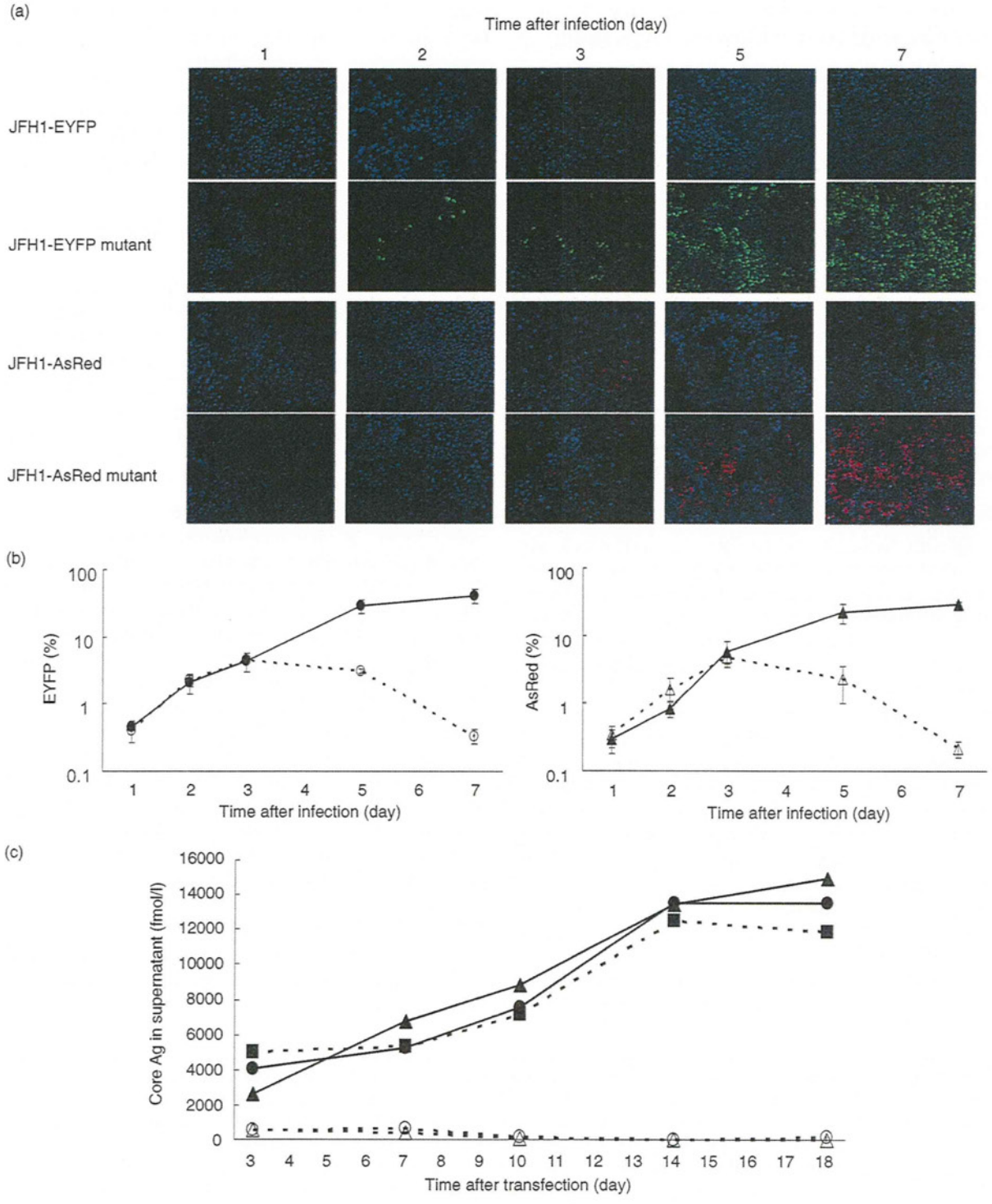

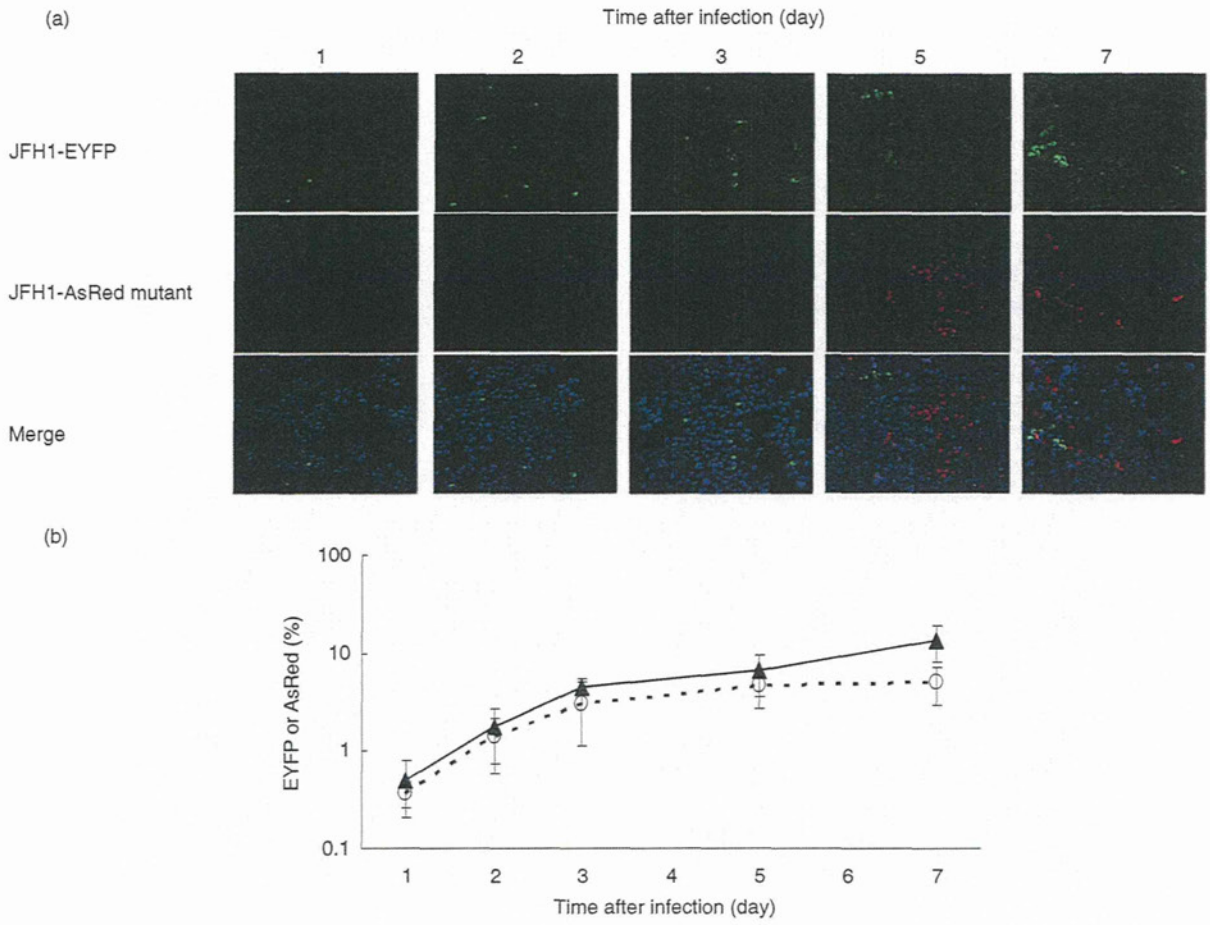

Figure 3 Intracellular *trans*-complementation of virus proteins. (a) Culture media from JFH1-EYFP and JFH1-AsRed mutant-transfected cells at 3 days post-transfection were added onto uninfected Huh7.5.1 cells. At the days indicated, EYFP or AsRed-directed-fluorescence was visualized directly. (b) The ratio of EYFP or AsRed-positive cells in Fig. 2a is calculated and plotted vs time. Assays were carried out in triplicate and the results are expressed as mean ± standard deviation. —▲— JFH1-AsRed mutant; ···◇··· JFH1-EYFP.

RESULTS

Infectious HCV reporter virus with robust virus production capability

FIRST, WE STUDIED whether the JFH1-EYFP mutant viruses are able to secrete sufficient amounts of infectious virus particles. Full-length HCV RNA was transcribed *in vitro* and transfected into Huh7.5.1 cells. Culture media were collected from cells transfected with JFH1-EYFP, JFH1-EYFP mutant, JFH1-AsRed, or JFH1-AsRed mutant, respectively, and inoculated into uninfected Huh7.5.1 cells. EYFP- or AsRed-positive cells were

Figure 4 Localization and expression of NS5A-EYFP and NS5A-AsRed fusion proteins. (a,b) Huh7.5.1 cells transfected with JFH1-EYFP, AsRed and their mutant RNA genomes were fixed at 3 days post-transfection. NS5A-EYFP and NS5A-AsRed fusion proteins were visualized using EYFP and AsRed, respectively. DsRed auto-fluorescence was observed directly. NS5A and core proteins were immunostained with Alexa Fluor 488-labeled goat antimouse immunoglobulin G (green). 4′,6′-diamidino-2-phenylindole dihydrochloride (DAPI) (blue) staining revealed the nuclear chromatin. Bars represent 10 μm. (c) Cells were transfected with EGFP, JFH1, JFH1-EYFP, JFH1-AsRed, JFH1-EYFP mutant or JFH1-AsRed mutant. Cells were harvested at 3 days post-transfection, and western blotting was performed by using anti-GFP, NS5A or core antibodies.

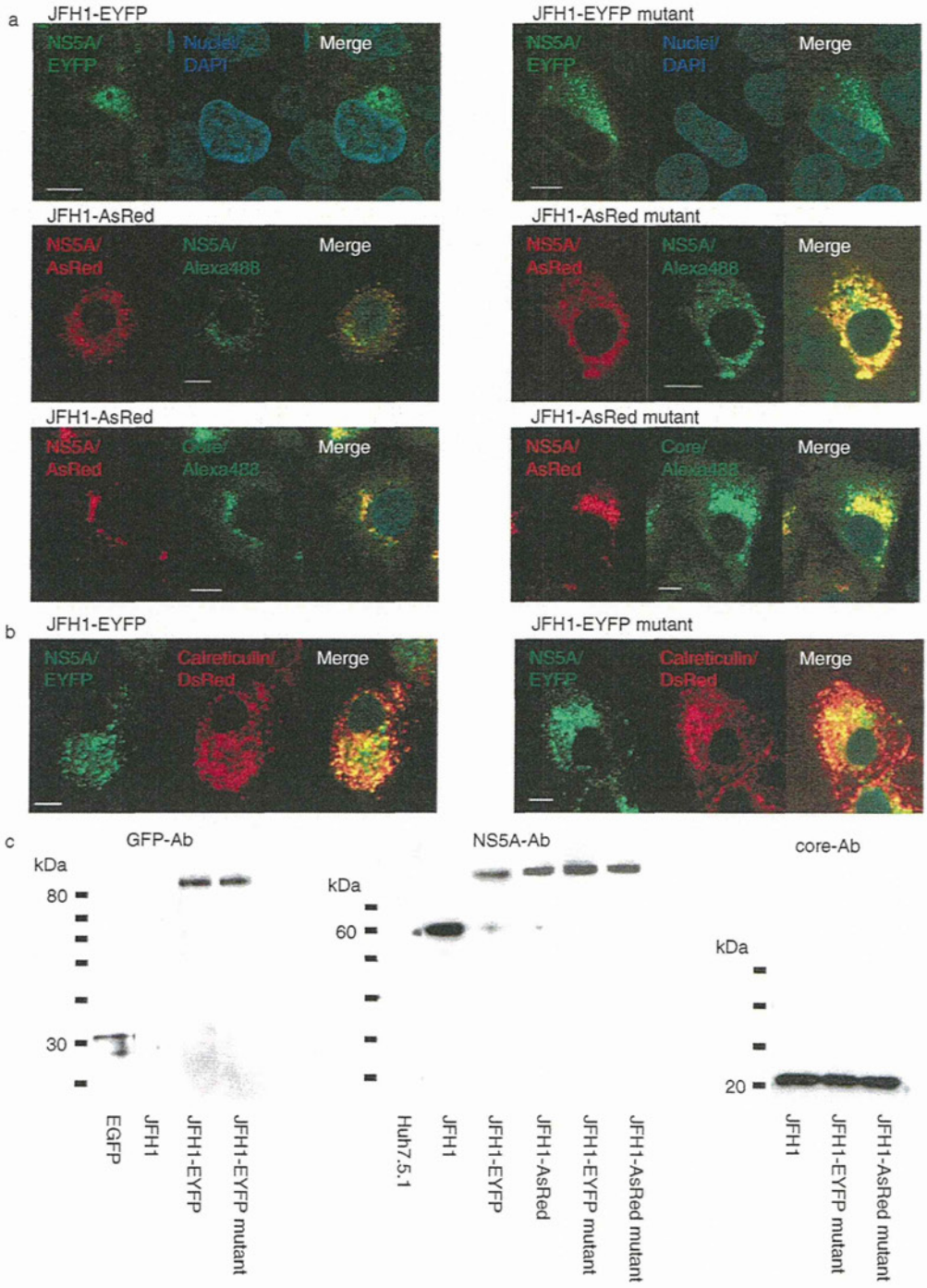

directly visualized by fluorescence microscopy on days 1–7. As shown in Figure 2(a), the number of cells positive for both JFH1-EYFP and JFH1-AsRed mutants, but not for JFH1-EYFP and JFH1-AsRed-infected cells, increased in a time-dependent manner. In JFH1-EFYP mutant-transfected cells, the proportion of EYFP-positive cells on days 3, 5 and 7 post-infection was 4.4%, 29% and 41%, respectively. In contrast, only 4.9% of JFH1-EYFP-transfected cells became EYFP-positive at 3 days post-infection, and the percentage of these fluorescence-positive cells decreased rapidly thereafter (Fig. 2b). Similarly, the percentage of cells infected with JFH1-AsRed mutant but not JFH1-AsRed increased exponentially. These results indicated that the two fluorescence virus clones with mutations are able to secrete infectious virus particles. We next compared levels of HCV core antigen in culture medium of cells infected with JFH1, JFH1-EYFP, JFH1-EYFP mutant, JFH1-AsRed, and JFH1-AsRed mutant viruses. The mutant viruses, but not the wild-type, produced amounts of core protein comparable to that of the parental JFH1 (Fig. 2C). In HCV-JFH1, JFH1-EYFP mutant, and JFH1-AsRed mutant-transfected cells, the core protein reached a peak of 1.25, 1.35 and 1.34 fmol/L, respectively, at 14 days post-transfection, while that of JFH1-EYFP JFH1-AsRed-transfected cells became undetectable at 10 days post-transfection. These results indicated that the mutant type is capable of producing an amount of viral particles comparable to that of the parental JFH1.

Using the two fluorescence-tagged viruses, we conducted co-infection of two virus strains, JFH1-AsRed mutant, which secreted infectious virus particles, and JFH1-EYFP, in which virus particle secretion was impaired. We collected culture media from cells transfected with JFH1-AsRed-mutant or JFH1-EYFP on day 2 post-transfection and infected both media onto uninfected Huh7.5.1 cells at a multiplicity of infection (moi, focus forming unit per cell) of 0.01. The number of JFH1-AsRed mutant-infected cells increased exponentially until day 3 but reached a plateau on days 5 and 7 post-infection. Interestingly, the number of cells positive for viral secretion-impaired JFH1-EYFP also increased in a manner similar to that of the JFH1-AsRed mutant (Fig. 3a). The percentage of AsRed mutant-positive cells was 4.6%, 6.7% and 14.8% at days 3, 5 and 7, respectively, while the percentage of EYFP-positive cells at the corresponding days was 3.1%, 4.8% and 5.1%, respectively (Fig. 3b). These results suggest that, in the co-culture of two HCV clones with and without virus particle secretion, a secretion-impaired virus clone is able to replicate and produce infectious particles possibly through the complementation of the intact virus.

Expression and subcellular localization of NS5A-fluorescence proteins

We next used fluorescence microscopy to study the subcellular localization of fluorescence and viral proteins. In cells transfected with JFH1-EYFP, JFH1-AsRed, and the respective mutants, EYFP and AsRed, were clearly visualized as dot-like structures in the perinuclear area (Fig. 4a). To determine if the NS5A-AsRed fusion protein indicates the subcellular localization of NS5A, we performed immunofluorescence staining of JFH-AsRed- and JFH1-AsRed mutant-infected cells using NS5A and HCV-core antibodies. Fluorescence of AsRed was co-localized precisely with NS5A and partially with core proteins. The fluorescence intensities of the JFH1-EYFP and -AsRed mutants within the cells were equal to that of the wild-type constructs. EYFP-NS5A of wild type and mutant JFH1 were localized in the ER (Fig. 4b). Western blotting was performed by using anti-GFP and anti-HCV-NS5A antibodies. As shown in Figure 4(c), three bands of the expected molecular weights of 27, 58 and 85 kDa, which corresponded to EGFP, NS5A and NS5A-EYFP fusion protein, were detected in EGFP, JFH1, JFH1-EYFP, JFH1-AsRed, JFH1-EYFP mutant, and JFH1-AsRed mutant-transfected cells. The expression levels of core protein in JFH1-EYFP mutant- and JFH1-AsRed mutant-transfected cells were almost the same as those transfected with parental JFH1. These results indicate

Figure 5 Kinetics of hepatitis C virus (HCV)-infected cells. (a) Huh7.5.1 cells were infected with JFH1-EYFP or JFH1-EYFP mutant HCV RNA. At the days indicated, cells were harvested and subjected to flow cytometry. EYFP-positive cells were sorted based on EYFP activating (*x*-axis) and staining with a marker of dead cells (*y*-axis). The results are depicted as density plots. The ratios of EYFP-positive cells vs time are shown below. Assays were carried out in triplicate and the results are expressed as mean ± standard deviation. $^{*}P < 0.05$. $^{**}P < 0.01$. —•—, JFH1-EYFP mutant; ·◇·, JFH1-EYFP. (b) Culture media from JFH1-EYFP or mutant-transfected cells were added onto uninfected Huh7.5.1 cells at a moi of 0.01. At the days indicated, infected cells were analyzed using flow cytometry. The results are depicted as density plots. The ratio of EYFP-positive cells vs time are shown below. Assays were carried out in triplicate and the results are expressed as mean ± standard deviation. $^{*}P < 0.05$. $^{**}P < 0.01$. WT, wild type. —•—, JFH1-EYFP mutant; ·◇·, JFH1-EYFP.